coatings

Article

The Laser Alloying Process of Ductile Cast Iron Surface with Titanium Powder in Nitrogen Atmosphere

Aleksandra Lont [1,*], Jacek Górka [1], Damian Janicki [1] and Krzysztof Matus [2]

[1] Welding Department, Faculty of Mechanical Engineering, Silesian University of Technology, Konarskiego Street 18A, 44-100 Gliwice, Poland; jacek.gorka@polsl.pl (J.G.); damian.janicki@polsl.pl (D.J.)
[2] Materials Research Laboratory, Faculty of Mechanical Engineering, Silesian University of Technology, Konarskiego Street 18A, 44-100 Gliwice, Poland; krzysztof.matus@polsl.pl
* Correspondence: aleksandra.lont@polsl.pl

Abstract: The article presents the results of the laser alloying process of a ductile cast iron EN-GJS 350-22 surface with titanium powder in nitrogen atmosphere. The aim of this research was to test the influence of nitrogen atmosphere on the structure and properties of the ductile cast iron surface layer produced by a laser alloying process with titanium. The laser alloying process was conducted using a Rofin Sinar DL020 2 kW high-power diode laser (HPDDL) with rectangular focus and uniform power density distribution in the focus axis. The tests of the produced surface layers included macrostructure and microstructure observations, X-ray diffraction (XRD) analysis, energy-dispersive spectroscopy (EDS) on scanning electron microscope (SEM) and transmission electron microscope (TEM), Vickers hardness and solid particle erosion according to ASTM G76-04 standard. As a result of the laser alloying process in nitrogen atmosphere with titanium powder, the in situ metal matrix composite structure reinforced by TiCN particles was formed. The laser alloying process of ductile cast iron caused the increased hardness and erosion resistance of the surface.

Keywords: laser alloying; ductile cast iron; metal matrix composite; solid particle erosion

check for updates

Citation: Lont, A.; Górka, J.; Janicki, D.; Matus, K. The Laser Alloying Process of Ductile Cast Iron Surface with Titanium Powder in Nitrogen Atmosphere. *Coatings* **2022**, *12*, 227. https://doi.org/10.3390/coatings12020227

Academic Editor: Jinyang Xu

Received: 19 January 2022
Accepted: 8 February 2022
Published: 10 February 2022

1. Introduction

Ductile cast irons (DCIs) are alloys commonly used in industrial applications due to their high mechanical and fatigue strengths, plastic properties, low stress-concentration tendency, vibration-damping abilities and good casting properties and machinability, which make these materials relatively cheap and easy to form, even into complex shapes [1–3]. However, for some applications where the machine parts are operating under wear conditions, ductile cast irons exhibit insufficient wear resistance. For this purpose, surface engineering technologies are used to improve the wear resistance of the surface, while maintaining the beneficial mechanical and plastic properties of the ductile cast iron core. For these alloys, laser surface treatment technologies are commonly used [4–8].

The use of a laser beam for surface treatment of materials has many beneficial properties, such as rapid heating and cooling, which contributes to the formation of unique structures of surface layers or coatings and causes low heat impact on the base material structure and low deformation. Moreover, the laser beam can be used for precise surface treatment of even small areas with high efficiency [9,10]. Among the laser surface treatment technologies, laser surface transformation hardening, laser surface melting, laser surface alloying and laser cladding are mainly used. In the case of ductile cast irons, laser surface melting and alloying are most commonly used. The laser surface melting process of DCI surface causes up to 4 times surface hardness increase and has a beneficial effect on the tribological and erosive wear resistance [11–14]. The increased properties of laser-melted ductile cast iron surface are related to the microstructure change of the surface layer, in which during the melting process, the graphite dissolves in the liquid metal, leading to carbon enrichment of metal pool. During rapid cooling the carbon precipitates as cementite [15].

The laser surface alloying process in comparison to laser melting allows for a wider influence on the structure and properties of surface layers by adjusting the chemical composition of a liquid metal pool by the addition of the alloying elements. Previous studies in this field have shown that the addition of elements with high affinity to carbon in the laser alloying process may result in the formation of an in situ composite structure in the surface layer area [16–19]. An example of such an element is titanium, which when added in the laser alloying of a ductile cast iron surface causes the formation of high-hardness titanium carbides in the structure of the surface layer, which has a beneficial effect on the wear resistance of the surface. Research in the field of laser alloying of ductile cast irons with titanium has shown that with the appropriate selection of process parameters, it is possible to produce homogeneous surface layers and control their structure and properties, including the fraction, size and morphology of titanium carbides [20–25].

Titanium, besides high affinity to carbon, also has a high affinity to nitrogen and can form titanium nitrides and carbonitrides, which, like carbides, exhibit high hardness and can reinforce the composite structure for high wear resistance [25,26]. Many studies on titanium surface nitriding have been conducted, and the results are available in the literature [27,28], while only a few studies have been conducted on ductile cast iron surface alloying with titanium and nitrogen [29]. In the available research in this field [29], Si_3N_4 was used as the source of nitrogen in the alloying process, and no titanium carbonitrides were found in the produced surface layers. The research presented in this work was aimed at carrying out the laser alloying process of ductile cast iron surface with titanium powder in nitrogen shielding in order to form the in situ composite surface layer structure reinforced by titanium carbonitrides. The research included macrostructure and microstructure analysis, hardness measurements and solid particle erosion tests, and it aimed to determine the impact of the laser surface alloying process used on the structure and properties of the surface layer.

2. Materials and Methods

The EN-GJS-350-22-grade ductile cast iron (Bumar-Łabędy S.A., Gliwice, Poland) was used as a base material for the research. The chemical composition of the ductile cast iron used is presented in Table 1 and its microstructure is presented in Figure 1. The base material structure is composed of a ferritic matrix with about 20 vol.% of spheroidal graphite precipitates with an average diameter of 65 µm. The substrate surface was prepared before the laser alloying process by grinding to surface finish R_a of 0.5 µm and degreased with 95% ethyl alcohol.

Table 1. The ductile cast iron EN-GJS-350-22 chemical composition.

Chemical Composition, wt.%								
C	**Si**	**Mn**	**P**	**S**	**Cu**	**Ti**	**Mg**	**Cr**
3.66	2.71	0.527	0.042	0.001	0.068	0.032	0.012	0.124

For the laser alloying process, the 99.0% pure titanium powder H.C. Starck Amperit 154 with 45–70 µm gradation and 99.999% pure nitrogen were used. The titanium powder was dried at 50 °C for 30 min before the alloying process.

The laser surface alloying process was carried out using a Rofin Sinar DL020 high-power diode laser (HPDDL, Rofin-Sinar Laser GmbH, Hamburg, Germany) (Table 2) with a direct beam transmission to the material surface. The rectangular laser beam focus with dimensions of 1.5 mm × 6.6 mm was characterized by a uniform density distribution along the focus axis. The laser beam was focused on the base material surface. The station was also equipped with a numerically controlled positioning system for the laser head and base material. The movement of the traverse was parallel to the short axis of the laser beam focus. For the powder feeding, a disk powder feeding system with a vibrator was used. The titanium powder was fed directly into the area of laser beam impact at an angle of 45°

to the substrate surface. The powder nozzle shape and size were adapted to laser beam focus shape and size in order to ensure uniform powder injection. Nitrogen was used as powder transporting gas with the flow rate of 3 L/min and as a shielding gas with the flow rate of 15 L/min. For the research, single laser-alloyed beads were produced. The process parameters included laser beam power of 1500, 1750 and 2000 W; powder feed rate of 4, 5.33, 6.67 and 8 mg/mm; and process speed of 0.075 m/min (Table 3). The laser surface alloying process was carried out without preheating the substrate.

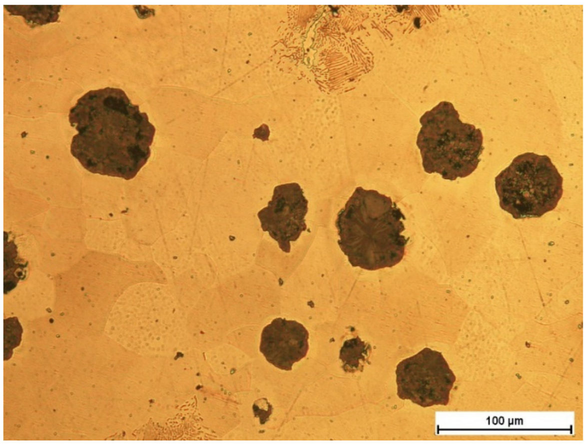

Figure 1. The ductile cast iron EN-GJS-350-22 microstructure (optical microscope).

Table 2. Technical specifications of the Rofin Sinar DL020 HPDDL.

Wavelength of the Laser Radiation, nm	808–940 ± 5
Range of Laser Power, W	100–2000
Focal Length, mm	82
Laser Beam Spot Size, mm	1.5 × 6.6
Range of Laser Power Intensity, W/mm^2	10.1–202.0

Table 3. The laser surface alloying process parameters.

Designation	Laser Beam Power, W	Traverse Speed, m/min	Powder Feed Rate *, mg/mm
Ti-N1	1500	0.075	4
Ti-N2	1500	0.075	5.33
Ti-N3	1500	0.075	6.67
Ti-N4	1500	0.075	8
Ti-N5	1750	0.075	4
Ti-N6	1750	0.075	5.33
Ti-N7	1750	0.075	6.67
Ti-N8	1750	0.075	8
Ti-N9	2000	0.075	4
Ti-N10	2000	0.075	5.33
Ti-N11	2000	0.075	6.67
Ti-N12	2000	0.075	8

* Powder feed rate is given as the powder weight (in mg) per 1 mm of bead.

The macroscopic analysis included macrostructure observations, measurements of bead cross-section geometrical parameters (width, depth and area) and uniformity analysis. The macrostructure observations of processed surface layers were carried out using an Olympus SZX9 optical stereoscopic microscope (Olympus, Tokyo, Japan). The geometrical parameters of the bead cross-sections (width, depth and area) were measured using macrographs in AutoCAD 2018 software (version 22.0). In order to determine the uniformity of the distribution of in situ formed precipitates, observation on a Phenom-World PRO scanning electron microscope (SEM, Thermo Fisher Scientific, Waltham, MA, USA) was carried out on the bead cross-sections on nonetched specimens in four areas near the surface and four areas near the fusion line. The average TiCN precipitate fractions were measured in those areas using Image-Pro Plus software (version 4.5.0.29), and surface energy-dispersive spectroscopy (EDS) analysis was conducted to determine the average titanium content. The laser-alloyed surface layers with over 30% relative standard deviations of the TiCN precipitate fraction and titanium content results, together with the surface layers in which the TiCN precipitate aggregates were observed, were discarded from further research as nonuniform.

The microscopic analysis included microstructure observations on a scanning electron microscope and a transmission electron microscope (TEM) together with EDS analysis and X-ray diffraction (XRD) analysis. The microstructure observations and EDS analysis were carried out using Phenom-World PRO scanning electron microscope and FEI TITAN 80/300 transmission electron microscope (Scientific and Technical Instruments, Hillsboro, OR, USA). The thin foil for TEM observations was prepared using Xe-PFIB technology. The XRD analysis on previously ground laser-alloyed surface layers was carried out on a PANalytical X'Pert PRO MPD diffractometer (Malvern Panalitycal, Malvern, UK) equipped with PIXcel3D 1×1 detector using filtered radiation from the lamp with cobalt anode. The fraction of the cementite in the structure was measured using Image-Pro Plus software (version 4.5.0.29).

The Vickers hardness was measured for each surface layer in cross-section with a load of 200 g and dwell time of 10 s using a Wilson Wolpert 401 MVD tester (Wilson Instruments, Instron Company, Norwood, MA, USA). The hardness measurements were conducted in three measuring lines from the surface to base material with 0.1 mm step (Figure 2).

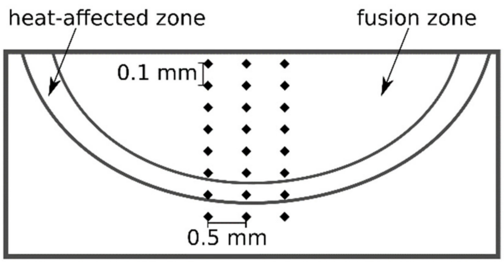

Figure 2. The Vickers hardness measurement point distribution on the cross-sections of laser-alloyed beads.

The solid particle erosion tests of homogeneous laser-alloyed surface layers and the base material surface were conducted on a test stand that met the requirements of the ASTM G76-04 standard [30]. The erodent material used for the test was angular 50 µm Al_2O_3 in a stream of dry compressed air. The erodent velocity was 70 m/s, and the feed rate was 2 g/min. The erodent was injected for 10 min on the tested material surface using a nozzle with a diameter of 1.5 mm and length of 50 mm. The distance between the nozzle and material surface was 10 mm. The solid particle erosion tests were carried out for impingement angles of 30° and 90° (for each angle and material, three tests were carried out). As a result of solid particle erosion tests, the mass loss was obtained using a laboratory scale with 0.001 g accuracy. The tested surface layers and base material densities were determined using the Archimedes method. As test results, the erosion rate and erosion value were counted in accordance with the ASTM G76-04 standard. In order to determine the erosive wear mechanism, SEM microscopic observations of the crater surfaces were carried out.

3. Results

3.1. The Macroscopic Analysis

The macrostructure of the cross-section of the representative laser-alloyed surface layer is presented in Figure 3. The shape of the fusion zones of laser-alloyed surface layers is hemispherical, which results from the fact that the main mechanism of the fluid flow during the laser alloying process is the surface tension gradient (Marangoni convection). The fusion shape indicates that the highest surface tension was in the central area of the molten pool. The results of bead depth, width and cross-section area measurements are presented in Table 4. On the basis of these results, it was found that with the constant laser beam power, the increased titanium powder feed rate had a negligible effect on the beads' width, depth and cross-section area. The increase in the laser beam power with a constant process speed and powder feed rate resulted in a slight increase in bead width, depth and cross-section area, due to higher heat input.

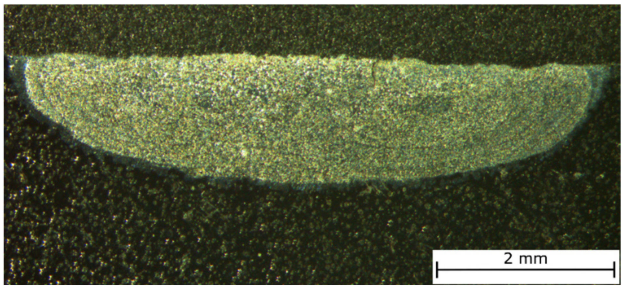

Figure 3. The macrostructure of the representative laser-alloyed surface layer.

Table 4. The laser-alloyed beads' depth, width and cross-section area measurements results (designation in accordance with Table 3).

Designation (According to Table 3)	Bead Width, mm	Bead Depth, mm	Bead Cross-Section Area, mm^2
Ti-N1	6.3 ± 0.12	1.4 ± 0.11	6.4 ± 0.12
Ti-N2	6.3 ± 0.1	1.4 ± 0.08	6.7 ± 0.18
Ti-N3	6.4 ± 0.16	1.5 ± 0.07	6.1 ± 0.22
Ti-N4	5.8 ± 0.13	1.1 ± 0.05	4.6 ± 0.15
Ti-N5	6.4 ± 0.11	1.4 ± 0.07	6.9 ± 0.25
Ti-N6	6.4 ± 0.2	1.5 ± 0.1	7.0 ± 0.23
Ti-N7	6.4 ± 0.1	1.7 ± 0.1	7.5 ± 0.16
Ti-N8	6.1 ± 0.13	1.3 ± 0.08	5.9 ± 0.18
Ti-N9	6.6 ± 0.19	1.4 ± 0.07	8.2 ± 0.13
Ti-N10	6.6 ± 0.12	1.6 ± 0.1	7.4 ± 0.2
Ti-N11	6.8 ± 0.15	1.9 ± 0.12	8.9 ± 0.19
Ti-N12	6.5 ± 0.1	1.4 ± 0.1	8.0 ± 0.21

As a result of the laser alloying process, titanium powder introduced into the liquid metal resulted in the formation of an in situ composite structure. Based on the relative standard deviations of titanium content and TiCN precipitate fraction, out of all produced laser-alloyed surface layers, three were qualified as homogeneous: Ti-N6, Ti-N9 and Ti-N10 (designations according to Table 3). The average titanium content from EDS (SEM) and average TiCN precipitate fraction of homogeneous laser-alloyed surface layers are presented in Table 5. The applied laser alloying process parameters allowed for the production of surface layers with the maximum average titanium content of 5.82 wt.% and the maximum average TiCN precipitate fraction of 10.12 vol.%. With the increase in titanium content, the average TiCN precipitate fraction increased, which is due to the fact that in the analyzed thermodynamic system, the TiCN precipitates are formed first (the Gibbs free energy is the lowest) [31]. The EDS line-scan analysis (Figure 4) carried out on the cross-section of the beads also showed that the process caused the homogeneous introduction of both titanium and nitrogen throughout the depth of the beads, by the fluid flow caused by Marangoni convection.

Table 5. The average titanium contents and Fe_3C and TiCN precipitate fractions of homogeneous laser-alloyed surface layers.

Designation (According to Table 3)	Average Titanium Content, wt.%	Average TiCN Precipitate Fraction, vol.%	Average Fe_3C Fraction, vol.%
Ti-N6	3.62 ± 0.88	6.47 ± 1.71	33.4 ± 2.25
Ti-N9	3.15 ± 1.26	4.75 ± 1.57	34.4 ± 5.76
Ti-N10	5.82 ± 1.35	10.12 ± 2.23	27.1 ± 3.93

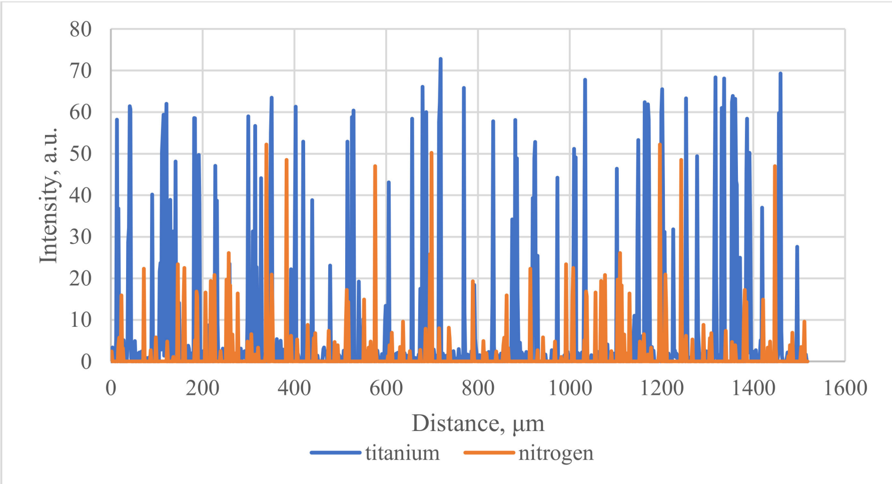

Figure 4. The titanium and nitrogen profile on the cross-section of a representative homogeneous laser-alloyed surface layer, from SEM/EDS line-scan analysis. Profile was taken in the center of the bead from surface to fusion line.

3.2. The Microscopic Analysis

The microstructures of the homogeneous laser-alloyed surface layers are presented in Figure 5. As a result of proceeded surface treatment, an in situ composite structure was formed in the surface layer. By heating the DCI surface with a laser beam, a thin surface layer was melted and the graphite precipitates dissolved in the liquid metal, causing the enrichment of the liquid metal with carbon. The additional enrichment of the molten pool with titanium powder and nitrogen during the laser alloying process caused the in situ formation of TiCN precipitates. Then, the TiCN precipitates were the crystal nucleus for primary austenite dendrites, and finally, the ledeburite was formed in the interdendritic spaces. The EDS mapping results (Figure 6) of the cross-section of the laser-alloyed surface layer indicate that the in situ formed precipitates are rich in carbon, titanium and nitrogen. Depending on the process parameters and titanium content, the morphology of the primary TiCN precipitates changes. In the case of surface layers with lower titanium content (3.15 wt.% and 3.62 wt.%), the morphology of TiCN precipitates is cubic, and with the increase in the titanium content to 5.82 the morphology changed to dendritic. The TEM EDS line-scan (Figure 7) proved that the precipitates are composed of carbon, titanium and nitrogen, and their chemical composition does not vary in the particle volume.

The fine-grained matrix is composed of primary austenite dendrites, partly after martensitic transformation, and ledeburite (with austenite partially transformed into martensite) in the interdendritic spaces. The matrix structure is a characteristic structure formed in the conditions of nonequilibrium cooling of liquid ductile cast iron, which was also obtained in the laser surface melting process [15]. The XRD analysis (Figure 8) confirmed the retained austenite occurrence in the surface layer structure. The cementite fraction (Table 5) decreased with the increase in titanium content and TiCN precipitate fraction, because during crystallization of the liquid metal pool, first the TiCN precipitates are formed, which is consistent with the results of thermodynamic calculations of the Fe-Ti-C-N system [31]. The high-angle annular dark-field scanning transmission electron microscopy (HAADF-STEM) observations (Figure 9) showed that the matrix of in situ composite laser-alloyed surface layer is composed of martensite laths and cementite. Additionally, the presence of nanometric plate-like secondary cementite precipitates was observed. The presence of such precipitates was also confirmed in the matrix structure of in situ composite surface layers of laser-alloyed ductile iron with titanium powder in an argon shield [32].

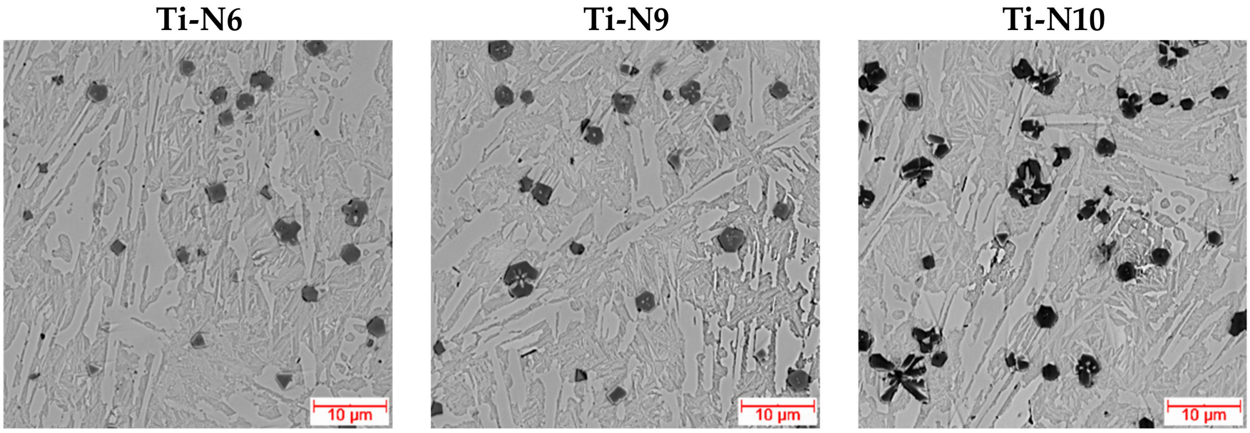

Figure 5. The microstructure of homogeneous laser-alloyed surface layers (designation according to Table 3).

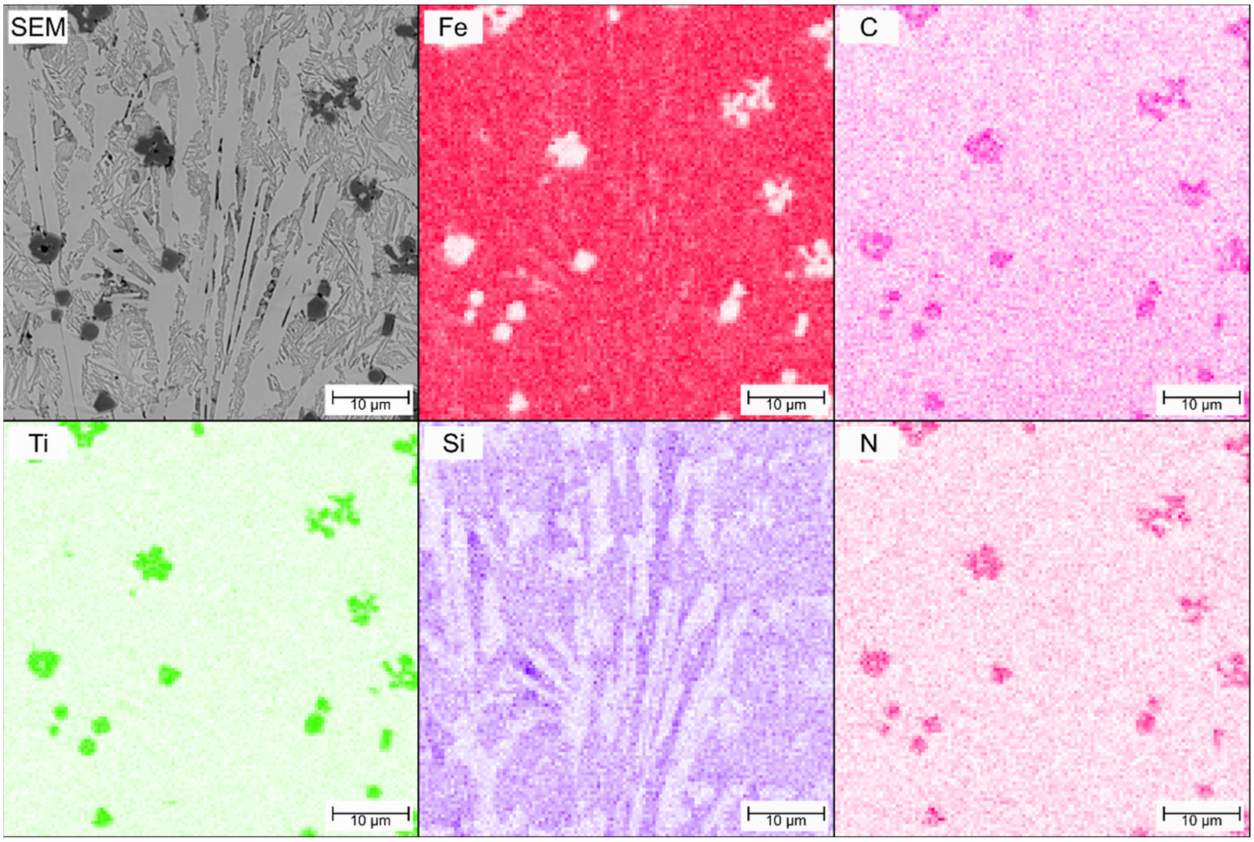

Figure 6. The EDS mapping of the composition of the representative laser-alloyed surface layer.

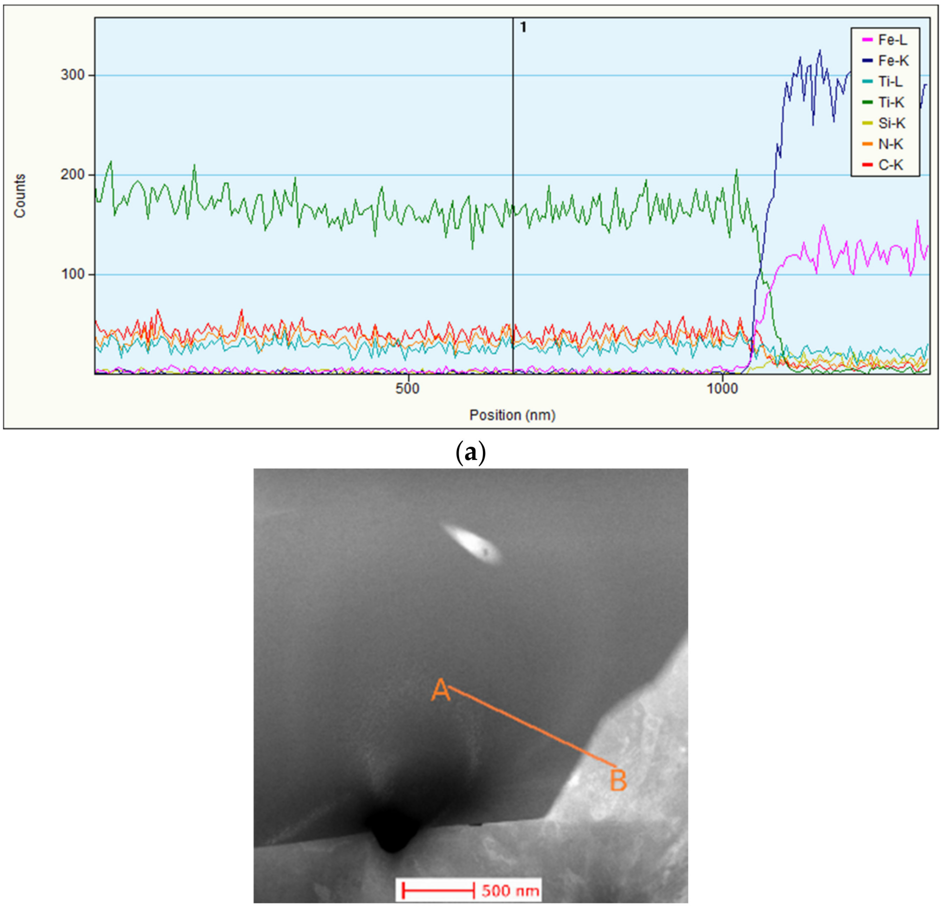

Figure 7. (**a**) The EDS line-scan profile of the composition of TiCN precipitate from TEM; (**b**) measuring line from A to B.

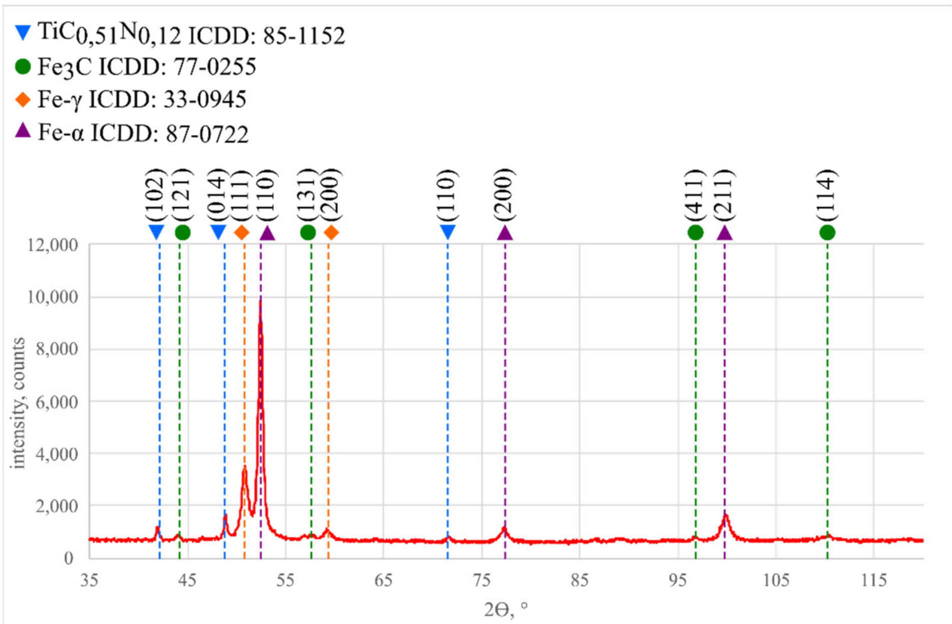

Figure 8. The XRD results of the representative homogeneous laser-alloyed surface layer.

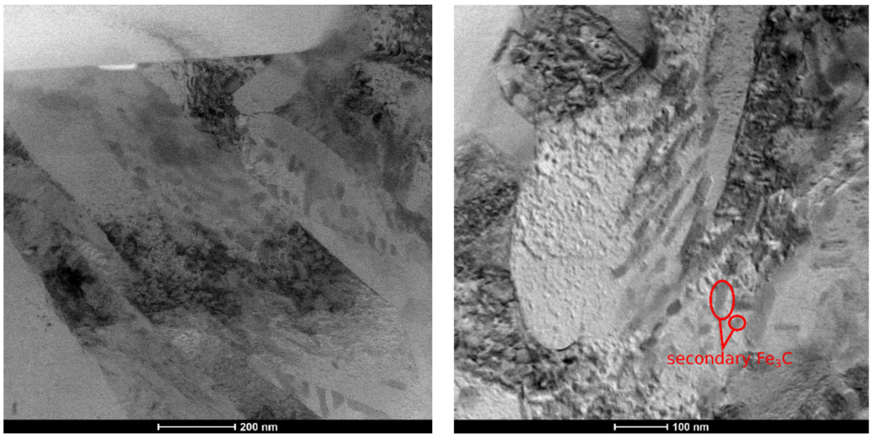

(**a**) (**b**)

Figure 9. The microstructure of the matrix of in situ composite laser-alloyed surface layer, HAADF-STEM. (**a**) is the matrix microstructure; (**b**) is the detailed view of the microstructure and the secondary Fe_3C.

3.3. The Hardness Tests

The Vickers hardness results are presented in Table 6 and Figure 10. The average hardness of homogeneous laser-alloyed surface layers depending on the process parameters, in comparison to the average base material hardness (235.9 HV0.2), increased by 166%–195%. With the increase in titanium content and TiCN precipitate fraction, the average hardness of the surface layers decreased, which is related to the decreased cementite fraction in the structure. The hardness depth profiles show that in the homogeneous laser-alloyed surface layers, hardness measurements are uniform along the entire depth of the fusion zone, and the hardness then decreases in the heat-affected zone and base material. The standard deviations of average hardness in each position in the heat-affected zone and base material are higher than those in the fusion zone due to the presence of low-hardness graphite precipitates.

Table 6. The average Vickers hardness results of homogeneous laser-alloyed surface layers.

Designation (According to Table 3)	Average Hardness, HV0.2
Ti-N6	663.2 ± 54.1
Ti-N9	695.7 ± 30.5
Ti-N10	626.9 ± 40.8

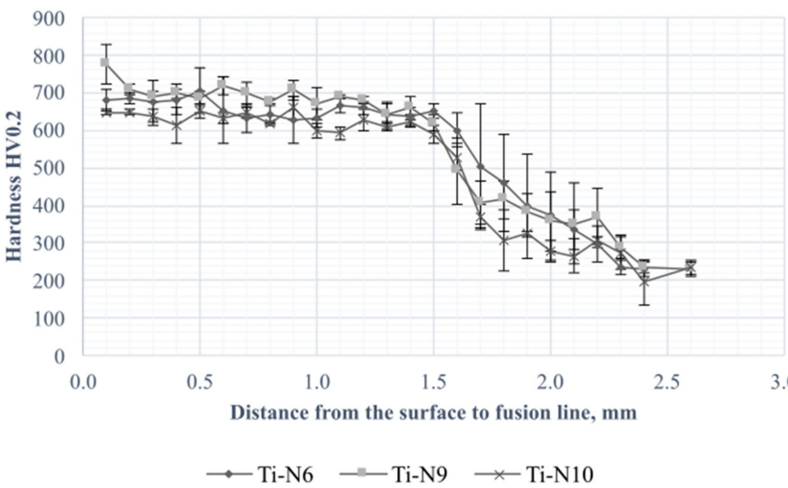

Figure 10. The Vickers hardness depth profiles of homogeneous laser-alloyed surface layers.

3.4. The Solid Particle Erosion Tests

The solid particle erosion test results are presented in Table 7. The laser alloying process of ductile cast iron surface with titanium powder in nitrogen shielding had a positive influence on increasing the erosion resistance of base material. In comparison to the DCI surface, the laser alloying process resulted in a decrease in the erosion value by a maximum of 33.4% for the impingement angle of 30° and by a maximum of 22.9% for the angle of 90°. The average erosion rates and values received for the impingement angle of 30° for each tested surface layer and base material are higher than those received for the impingement angle of 90°, which is characteristic of plastic materials [33]. For both tested impingement angles, out of the tested laser-alloyed surface layers, the highest erosion value was noted for the Ti-N9 surface layer (designation according to Table 3), which has the lowest Ti content and TiCN fraction. Together with the titanium content increase and average hardness decrease, the erosion value for both impingement angles slightly decreased.

Table 7. The solid particle erosion test results.

Designation (According to Table 3)	Density, g/cm^3	The Average Erosion Rate *, mg/min		The Average Erosion Value **, mm^3/g	
		Impingement Angle, °			
		30	90	30	90
Ti-N6	7.3	0.6 ± 0.05	0.39 ± 0.03	0.0411 ± 0.0031	0.0265 ± 0.0022
Ti-N9	7.3	0.55 ± 0.04	0.43 ± 0.04	0.0468 ± 0.0035	0.0368 ± 0.0037
Ti-N10	7.2	0.6 ± 0.03	0.38 ± 0.04	0.0414 ± 0.0021	0.0262 ± 0.0028
EN-GJS-350-22	7.1	0.88 ± 0.01	0.48 ± 0.05	0.0617 ± 0.0004	0.034 ± 0.0032

* erosion rate = mass loss (mg)/test time (min), ** erosion value = volume loss (mm^3)/total mass of erodent (g).

The SEM micrographs of crater surfaces after solid particle erosion tests are presented in Figure 11. The crater observations allowed the erosion mechanism of the tested surface layers and the base material to be specified. In the case of the reference DCI surface (Figure 11a,b), the plastic deformation (scars, grooves and craters) of the structure occurred during erosion under both investigated impingement angles, which allowed stating that the erosion mechanism was ductile. On the micrographs, the graphite precipitates can be observed. Additionally, the embedded erodent particles were observed on the crater surfaces. On the crater surfaces of laser-alloyed surface layers, the plastic deformation was also observed in the matrix material, but in this case, no embedded erodent particles were observed. The in situ formed high-hardness precipitates in the structure under the erosion conditions showed the brittle mechanism (cracks can be observed). In addition, voids were also observed in the crater surfaces, from which the TiCN precipitates were torn out during erosion. The erosion mechanism for the laser-alloyed composite surface layers is then different for the matrix and reinforcement material.

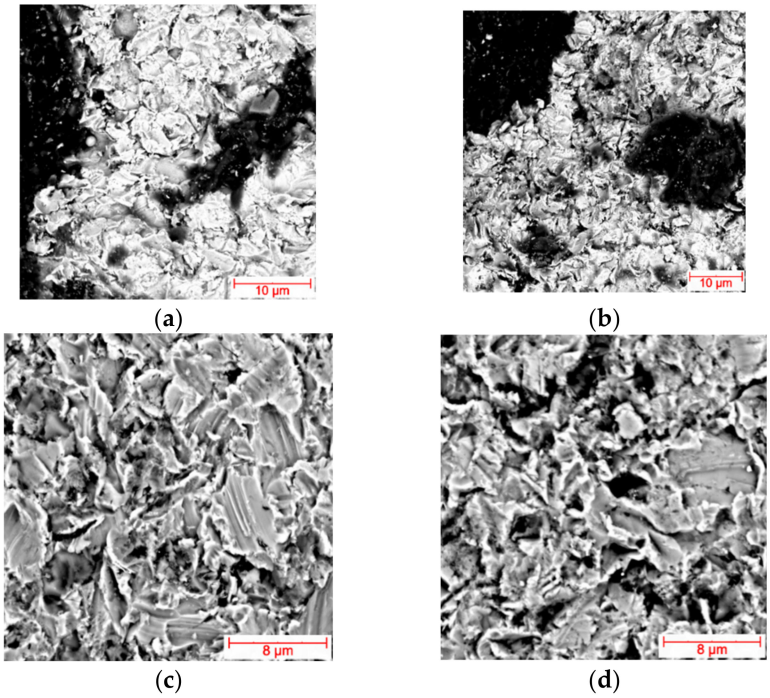

Figure 11. The SEM micrographs of craters surface after erosion test: (**a**) EN-GJS-350-22, impingement angle 30°; (**b**) EN-GJS-350-22, impingement angle 90°; (**c**) the representative laser-alloyed surface layer, impingement angle 30°; (**d**) the representative laser-alloyed surface layer, impingement angle 90°.

4. Conclusions

Based on the analysis of the achieved test results, the following conclusions have been reached:

1. The laser alloying process of the EN-GJS-350-22 ductile cast iron surface with titanium in nitrogen shielding allows for the formation of homogeneous in situ composite surface layers reinforced by TiCN precipitates.
2. During the laser alloying process of the DCI surface, the graphite dissolved in the molten pool, causing carbon enrichment. The addition of titanium and nitrogen in the process resulted in the metallurgical reaction of TiCN particle formation occurring uniformly in the molten pool. The applied process parameters allowed the production of homogeneous surface layers with a TiCN precipitate fraction of 4.75 ÷ 10.12 vol.%. Depending on the titanium content, the in situ formed TiCN precipitates show cubic or dendritic morphology. The chemical composition of TiCN precipitates is uniform in their depth.
3. The matrix microstructure of laser-alloyed surface layers is composed of primary austenite dendrites partially after martensitic transformation, the mixture of austenite (partially after martensitic transformation) and cementite in the interdendritic spaces and the nanometric secondary plate-like cementite precipitates. The eutectic cementite fraction in surface layers decreases with the increase in titanium content, due to the order of phase crystallization during cooling.
4. The laser alloying process of ductile cast iron surface resulted in an increase in the average hardness of the base material used by up to 195%. The average hardness decreased with the increase in titanium content, due to the decrease in cementite in the structure.
5. The solid particle erosion test results showed that the applied laser alloying process has a positive effect on the erosion resistance of base material, which increased by up to 33.4% and 22.9% for the impingement angles of 30° and 90°, respectively. The titanium content increase in the surface layer affects the increased erosion resistance of surface layers. The erosion mechanism of the base material is ductile, while in the

case of in situ composite surface layers, the matrix was plastically deformed and the TiCN precipitates showed brittle failure.

Future research will be focused on the elevation of titanium concentration in the melt by affecting the intensity of the fluid flow in the molten pool.

Author Contributions: Conceptualization, A.L., J.G. and D.J.; methodology, A.L., J.G. and D.J.; formal analysis, A.L., J.G. and D.J.; investigation, A.L., D.J. and K.M.; data curation, A.L. and K.M.; writing—original draft preparation, A.L.; writing—review and editing, D.J. and J.G. All authors have read and agreed to the published version of the manuscript.

Funding: This research received no external funding.

Institutional Review Board Statement: Not applicable.

Informed Consent Statement: Not applicable.

Data Availability Statement: Data sharing is not applicable to this article.

Conflicts of Interest: The authors declare no conflict of interest.

References

1. Elliot, R. *Cast Iron Technology*, 1st ed.; Butterworth & Co.: London, UK, 1988; pp. 13–20.
2. Durand-Charre, M. *Microstructure of Steels and Cast Irons*, 1st ed.; Springer: Berlin/Heidelberg, Germany, 2004; pp. 356–363.
3. Żuk, M.; Górka, J.; Dojka, R.; Czupryński, A. Repair welding of cast iron coated electrodes. *IOP Conf. Ser. Mater. Sci. Eng.* **2017**, *227*, 012139. [CrossRef]
4. Ayday, A.; Durman, M. Surface hardening of ductile cast iron by electrolytic plasma technology. *Acta Phys. Pol.* **2013**, *123*, 291–293. [CrossRef]
5. Li, C.; Guan, Q.; Cai, J.; Zhang, C.; Lv, P.; Jin, Y. Surface alloying of gray cast iron with chromium by high current pulsed electron beam treatment. *Mater. Res. Express* **2018**, *5*, 066518. [CrossRef]
6. Abboud, J.H. Microstructure and erosion characteristic of nodular cast iron surface modified by tungsten inert gas. *Mater. Des.* **2012**, *35*, 677–684. [CrossRef]
7. Mardaras, E.; Gonzalez-Martinez, R.; Bayon, R.; Nastac, L.; Mendez, S. Surface modification of ductile iron produced by an innovative in-situ casting technique. *Int. J. Cast Met. Res.* **2020**, *33*, 103–111. [CrossRef]
8. Dahotre, N.B. Laser surface engineering. *Adv. Mater. Process* **2002**, *160*, 35–39.
9. Górka, J.; Czupryński, A.; Zuk, M.; Adamiak, M.; Kopyść, A. Properties and structure of deposited nanocrystalline coatings in relation to selected construction materials resistant to abrasive wear. *Materials* **2018**, *11*, 1184. [CrossRef] [PubMed]
10. Kusinski, J.; Kac, S.; Kopia, A.; Radziszewska, A.; Rozmus-Górnikowska, M.; Major, B.; Major, L.; Marczak, J.; Lisiecki, A. Laser modification of the materials surface layer—A review paper. *Bull. Pol. Acad. Sci.* **2012**, *60*, 711–728. [CrossRef]
11. Kotarska, A.; Janicki, D.; Górka, J.; Poloczek, T. Solid particle erosion of laser surface melted ductile cast iron. *Arch. Foundry Eng.* **2020**, *20*, 105–111.
12. Pagano, N.; Angelini, V.; Ceschini, L.; Campana, G. Laser remelting for enhancing tribological performances of a ductile iron. *Procedia CIRP* **2016**, *41*, 987–991. [CrossRef]
13. Murakami, R.; Narita, I.; Miyahara, H. Surface microstructure and properties of nodular cast iron rapidly solidified by laser surface melting. *Mater. Trans.* **2018**, *59*, 1465–1470. [CrossRef]
14. Chmielewski, T.; Hudycz, M.; Krajewski, A.; Sałaciński, T.; Skowrońska, B.; Świercz, R. Structure investigation of titanium metallization coating deposited onto AlN ceramics substrate by means of friction surfacing process. *Coatings* **2019**, *9*, 845. [CrossRef]
15. Janicki, D.; Górka, J.; Kwaśny, W.; Pakieła, W.; Matus, K. Influence of solidification conditions on the microstructure of laser-surface-melted ductile cast iron. *Materials* **2020**, *13*, 1174. [CrossRef] [PubMed]
16. Janicki, D. Farbication of high chromium white iron surface layers on ductile cast iron substrate by laser surface alloying. *Strojniski Vestn. J. Mech. Eng.* **2017**, *63*, 705–714.
17. Czupryński, A.; Mele, C. Properties of flame spraying coatings reinforced with particles of carbon nanotubes. *Adv. Mater. Sci.* **2021**, *21*, 56–76. [CrossRef]
18. Subramanian, K.; Murugesan, S.; Mohan, D.G.; Tomków, J. Study on dry sliding wear and friction behaviour of Al7068/Si3N4/BN hybrid composites. *Materials* **2021**, *14*, 6560. [CrossRef]
19. Kotarska, A. Laser surface alloying of ductile cast iron with Ti + 5% W mixture. *Weld. Tech. Rev.* **2019**, *91*, 19–25. [CrossRef]
20. Janicki, D. Microstructural evolution during laser surface alloying of ductile cast iron with titanium. *Arch. Metall. Mater.* **2017**, *62*, 2423–2429. [CrossRef]
21. Kotarska, A. The laser alloying process of ductile cast iron surface with titanium. *Metals* **2021**, *11*, 282. [CrossRef]
22. Janicki, D. The friction and wear behaviour of in-situ titanium carbide reinforced composite layers manufactured on ductile cast iron by laser surface alloying. *Surf. Coat. Technol.* **2021**, *406*, 126634. [CrossRef]

23. Levi, G.; Kaplan, W.D.; Bamberger, M. Structure refinement of titanium carbonitride (TiCN). *Mater. Lett.* **1988**, *35*, 344–350. [CrossRef]
24. Chen, L.; Lengauer, W.; Dreyer, K. Advances in modern nitrogen-containing hardmetals and cermets. *Int. J. Refract. Hard. Met.* **2000**, *18*, 153–161. [CrossRef]
25. Gucwa, M.; Bęczkowski, R.; Winczek, J.; Wyleciał, T. The effect of type of welding sequence during hardfacing chromium cast iron for erosion resistance. *Arch. Foundry Eng.* **2017**, *17*, 51–54. [CrossRef]
26. Lukaszkowicz, K.; Sondor, J.; Paradecka, A.; Węgrzyn, T.; Tański, T. Structure and tribological properties of AlCrN + CrCN coating. *Coatings* **2020**, *10*, 1084. [CrossRef]
27. Lisiecki, A. Study of optical properties of surface layers produced by laser surface melting and laser surface nitriding of titanium alloy. *Materials* **2019**, *12*, 3112. [CrossRef]
28. Li, G.; Yao, X.; Wood, R.J.; Guo, J.; Shi, Y. Laser surface nitriding of Ti-6Al-4V alloy in nitrogen-argon atmospheres. *Coatings* **2020**, *10*, 1009. [CrossRef]
29. Paczkowska, M. The evaluation of nodular iron surface layer modification by laser alloying with nitrogen and titanium. *Arch. Mech. Technol. Autom.* **2013**, *33*, 33–43.
30. ASTM International. *ASTM G76-04, Standard Test Method for Conducting Erosion Tests by Solid Particle Impingement Using Gas Jets*; ASTM International: West Conshohocken, PA, USA, 2004.
31. Gorbachev, I.I.; Popov, V.V. Analysis of the solubility of carbides, nitrides and carbonitrides in steels using methods of computer thermodynamics: III. Solubility of carbides, nitrides and carbonitrides in the Fe-Ti-C, Fe-Ti-N and Fe-Ti-C-N systems. *Phys. Met.* **2009**, *108*, 484–495. [CrossRef]
32. Janicki, D. *Shaping the Structure and Properties of Surface Layers of Ductile Cast Iron by Laser Alloying*, 1st ed.; Wydawnictwo Politechniki Śląskiej: Gliwice, Poland, 2018; pp. 70–106.
33. Stachowiak, G.W.; Batchelor, A.W. *Engineering Tribology*, 4th ed.; Butterworth-Heinemann: Oxford, UK, 2014; pp. 551–556.